ICSO 2016

International Conference on Space Optics

Biarritz, France

18–21 October 2016

Edited by Bruno Cugny, Nikos Karafolas and Zoran Sodnik

James Webb Space telescope optical simulation testbed: experimental results with linear control alignment

Sylvain Egron

Charles-Philippe Lajoie

Vincent Michau

Aurélie Bonnefois

et al.

International Conference on Space Optics — ICSO 2016, edited by Bruno Cugny, Nikos Karafolas, Zoran Sodnik, Proc. of SPIE Vol. 10562, 1056225 · © 2016 ESA and CNES
CCC code: 0277-786X/17/$18 · doi: 10.1117/12.2296105

JAMES WEBB SPACE TELESCOPE OPTICAL SIMULATION TESTBED: EXPERIMENTAL RESULTS WITH LINEAR CONTROL ALIGNMENT.

Sylvain Egron[1,2,3], Charles-Philippe Lajoie[1], Vincent Michau[2], Aurélie Bonnefois[2], Clément Escolle[3], Lucie Leboulleux[1,2,3], Mamadou N'Diaye[1], Laurent Pueyo[1], Elodie Choquet[4], Marshall D. Perrin[1], Marie Ygouf[1], Thierry Fusco[2,3], Marc Ferrari[3], Emmanuel Hugot[3], and Rémi Soummer[1]

[1] Space Telescope Science Institute, 3700 San Martin Drive, Baltimore, MD 21218, USA. [2] ONERA, 29 Avenue de la Division Leclerc, 92320 Châtillon, France. [3] Aix Marseille Université, CNRS, LAM (Laboratoire d'Astrophysique de Marseille) UMR 7326, 13388, Marseille, France. [4] Jet Propulsion Laboratory, California Institute of Technology, 4800 Oak Grove Drive, MS 169-506, Pasadena, CA 91109, USA Hubble Fellow.

I. INTRODUCTION

The current generation of terrestrial telescopes has large enough primary mirror diameters that active optical control based on wavefront sensing is necessary. Similarly, in space, while the Hubble Space Telescope (HST) has a mostly passive optical design, apart from focus control, its successor the James Webb Space Telescope (JWST) has active control of many degrees of freedom in its primary and secondary mirrors. JWST's wavefront sensing and control (WFS&C) system will have to set the telescope into its alignment state after the deployment and maintain that alignment for the lifetime of the mission [1].

The wavefront sensing and control technologies chosen for the JWST have been substantially tested in simulation and experimentally. For that purpose, Ball Aerospace built a 1:6 scale mock up of JWST: The Testbed Telescope (TBT), which was used to achieve the necessary demonstrations of technology readiness in preparation for JWST [2,3]. But WFS&C development remains an ongoing process, with novel algorithms arising that may provide increased efficiency [4], useful contingency capabilities for JWST [5], aid in its long term optical maintenance [6], and may be valuable for future even larger segmented space telescopes [7]. Developing the JWST Optical Simulation Testbed (JOST) at the Space Telescope Science Institute (STScI) provides a platform to test and evaluate new algorithms for WFS&C, with possible applications to JWST or to future missions such as the proposed Large UV/Optical/IR Surveyor (LUVOIR). Moreover, this testbed will be helpful to develop staff expertise for JWST commissioning and operations reproducing various steps of the alignment. It is a supplement to existing verification and validation activities for independent cross-checks and novel experiments, not a part of the mission's critical path development process.

JOST is a simplified model of JWST, not an exact scaled model as in the case of the TBT. But it provides a close enough physical model so that the key optical aspects remain the same, especially for the degrees of freedom which are most relevant for maintenance over the life of JWST such as segment tilts and misalignments of the secondary relative to the primary. To meet that requirement, JOST is a three-lens anastigmat, a refractive analogue to JWST's three mirror anastigmat. A lens and aperture stop define JOST's entrance pupil, with segmentation provided by a segmented deformable mirror conjugated with that pupil (in the re-imaged pupil plane equivalent to where JWST's Fine Steering Mirror is located). JOST is designed to achieve similar quality image and image sampling as JWST at 2 microns (> 80% Strehl ratio, and Nyquist sampled) over a field equivalent to the NIRCam module, but at 633 nm wavelength.

This paper presents the first experimental results of the WFS&C on the testbed. Our group presented a general overview of JOST in Perrin et al. [8] "James Webb Space Telescope Optical Simulation Testbed I: Overview and First Results", hereafter Paper I. Its detailed optical design and several trade studies were presented in Choquet et al.[9] "James Webb Space Telescope Optical Simulation Testbed II. Design of a Three-Lens Anastigmat Telescope Simulator", hereafter Paper II. The experimental implementation of the WFS&C on the testbed is described in Egron et al. [10] "James Webb Space Telescope Optical Simulation Testbed III: First experimental results with linear-control alignment", hereafter Paper III.
Recent work has focused on the overall alignment of the lenses, with the segmented deformable mirror (DM) not included in the optical path, to allow test and development of the testbed's software infrastructure for multifield wavefront sensing and linear control using a full circular pupil rather than a segmented and hexagonal one. The segmented DM control software has been developed separately, and the segmented DM will be re-added to JOST once the linear control infrastructure has been validated for alignment of the three lenses based on multi-field sensing. We emphasize that one of the unique aspects of JOST is its ability to model arbitrary 5-

degree-of-freedom misalignments of the primary, secondary, and tertiary lens with respect to one another, which can result in field-dependent wavefront errors that may not be sensed on a single field point in some cases.
In §2, we will focus on the optical simulation and the motorization of the testbed. In §3, we describe the implementation of wavefront control (WFC) algorithm on JOST. In §4, we present the first results of the linear control of L2, integrating WFS&C.

II. Testbed description

A. Optical simulation

The optical simulation of JOST is done with the Zemax Optic Studio 2016 software. As an example, this software produced the layout of the optical design presented on Fig. 1. For more detailed explanations about the optical design and the trade studies, see Paper II. Including all the optical components of the testbed in the simulation gives us the possibility to analyze some vignetting effects, or the sensitivity of the off-axis parabola position on the alignment process.

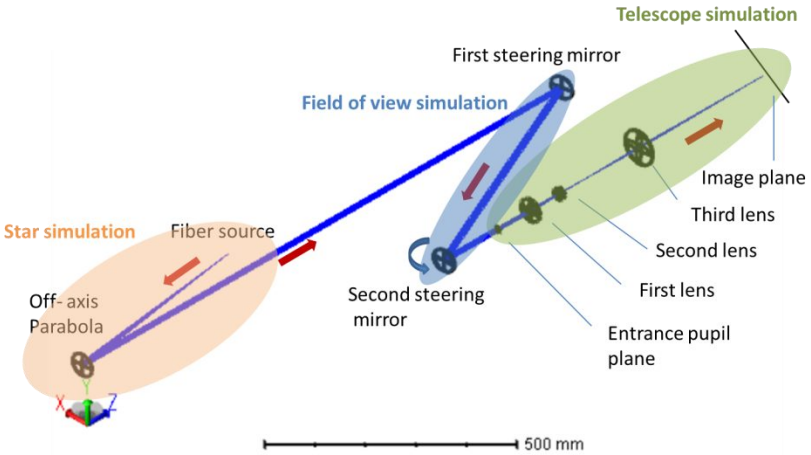

Fig. 1. Optical layout for JOST without DM (current state of the testbed). The fiber source simulates the flux of the star we are observing, the off-axis parabola collimates the beam. Actuators on the second steering mirror set the field of observation (the total field of view is 3.4˚x 3.4˚). The segmented DM will eventually be introduced in the exit pupil plane after the third lens.

B. Motorization of JOST

Since the purpose of JOST is to simulate the alignment of the primary and the secondary mirrors of JWST, motorized actuators are set to control the segmented mirror and the second lens of JOST:

- The primary mirror is an Iris AO MEMS deformable mirror, composed of 37 segments, which will be blocked down to 18 segments as in JWST. Each segment is controlled in piston, tip and tilt. We can control the deformable mirror through C++ software, in which the mirror configuration is defined by a 37 x 3 table that gives piston, tip and tilt values of each actuator. The segmented mirror and its software have been separately tested, but the mirror is not currently installed on the testbed. It will be added when the linear control infrastructure has been validated with the three lenses.
- The 5 degrees of freedom (tip, tilt and x, y, z positions) of the second lens are controlled by stepper actuators.

In addition, to make the automation of the testbed possible, the two axes (tip, tilt) of the steering mirror are motorized as well. Finally, since the WFS of JOST is handled by phase diversity algorithms, a translation stage allows the movement of the camera. The stepper actuators and the camera are controlled by software in Python.

C. Wavefront sensing for JOST

Our phase diversity software has been provided by ONERA. It is using a Maximum A Posterior estimator [11], [12] to extract the phase information from focus-diverse imagery. This estimator integrates a regularization on the aberrations based on Bayesian interpretation. We have experimentally tested the WFS methods, and validated the WFC algorithms compared to simulation in paper III.

III. Optical control model

Given the linearity properties of the optical design of JOST, we justify and develop the linear control model used for JOST.

A. Problem Statement

The optical control model consists in finding a relation between the wavefront observed and the alignment state of the testbed. To do so, we neglect the optical path change when a misalignment occurs. This is acceptable because, for JOST, the aberrations induced by the misalignments are lower than 300 nm rms. In this regime, the remaining aberrations of the system can be computed by summing the different phase maps representing the aberrations induced by each degree of freedom of L2. We can then define the wavefront as a function of the lens positions:

$$\phi(\theta) - \phi_0(\theta) = f_1^\theta(z) + f_2^\theta(x) + f_3^\theta(y) + f_4^\theta(\alpha) + f_5^\theta(\beta) \quad (1)$$

Where $\phi(\theta)$ is the wavefront of the system for an angular position θ, $\phi(\theta_0)$ is the wavefront of the system with L2 aligned (also called residual wavefront). $f_i^\theta(j)$ is the aberration induced by the misalignment of L2 along the degree of freedom i by the amount j for an angular position θ. We call f_i^θ the influence function for degree of freedom i and the angular position θ. z, x, y, α, β define the position of L2, they are equal to 0 when L2 is aligned.

The pupil of the system being a full circular aperture, we can project the wavefront observed onto the Zernike polynomial basis. We can constrain the resolution of equation (1) choosing different angular positions θ and different Zernike polynomials to project the wavefront on. Each of these projections is a sensing mode.

In the next part we look for sensing modes (the angular positions and Zernike polynomials) for which the projection of the functions f_1^θ, f_2^θ, f_3^θ, f_4^θ, f_5^θ are linear.

B. *Jacobian matrix of the system*

In the case of JOST, we can either compute the influence functions f_i^θ in simulation (using the software Zemax), or experimentally, moving L2 by small steps and measuring the wavefront each time. Fig.2 shows the comparison of the simulated and experimental influence functions $f_3^{\theta=1^\circ}$ and $f_4^{\theta=1^\circ}$. They are projected only on the polynomials Z_4 (defocus), Z_5 (oblique astigmatism), Z_6 (vertical astigmatism), Z_7 (vertical coma), Z_8 (horizontal coma). The contribution of other modes is very low and therefore too sensitive to the noise to be used as control modes.

The plots in Fig.2 show that $f_3^{\theta=1^\circ}$ and $f_4^{\theta=1^\circ}$ projected on Z_5, Z_7 and Z_8, are linear functions. Following the same process we have shown that this result is also true for the functions $f_1^{\theta=1^\circ}$, $f_2^{\theta=1^\circ}$ and $f_5^{\theta=1^\circ}$.

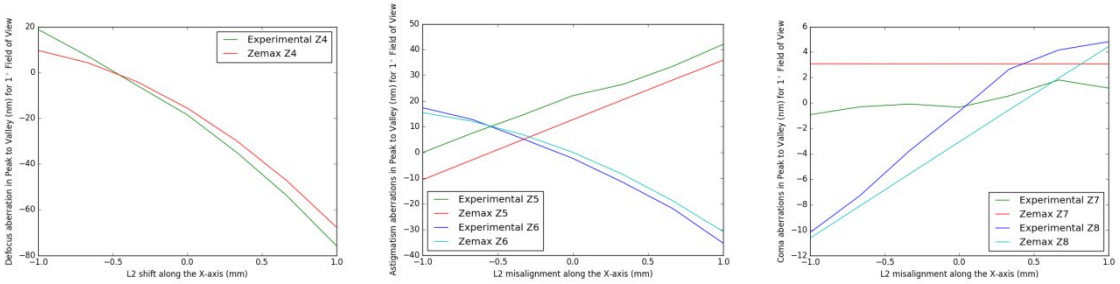

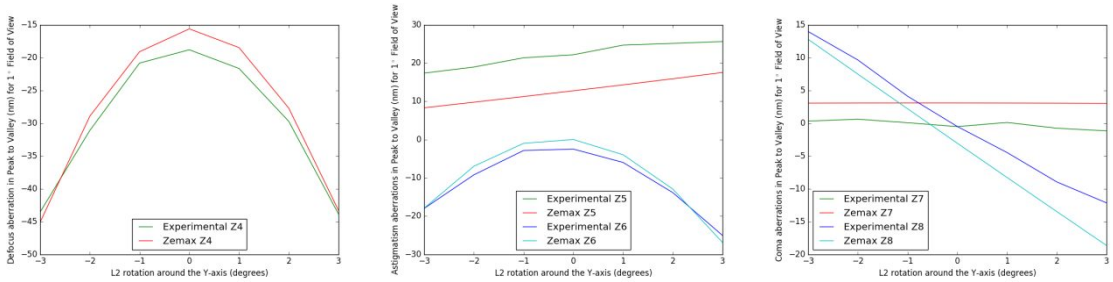

Fig. 2. Zernike coefficients (Z4, Z5, Z6, Z7 and Z8) as a function of lateral (upper plots) and tilt (lower plots) misalignment of L2 computed experimentally and in simulation. Z5, Z7 and Z8 modes are linear functions of misalignment amplitudes. Between experimental and simulation results the slopes of the plots are the same, the offset observed (smaller than 10 nm) corresponds to the wavefront errors of the testbed in its aligned state. Note that for 1˚ field of view, the defocus is a parabolic function of L2 rotation therefore it is not included in the control. On the other hand, on axis, defocus is very linear and by far the most sensitive aberration to a misalignment along the z-axis.

The projection of $f_3^{\theta=1^\circ}$ on Z_5 can be expressed as follow:

$$f_3^{\theta=1^\circ}(y)|Z_5(\theta=1^\circ) = \frac{\Delta Z_5(\theta=1^\circ)}{\Delta y} y + f_3^{\theta=1^\circ}(0) \qquad (2)$$

The linear control requires all the sensing modes chosen to be associated to linear influence functions [13,14]. In that case, (Eq. 1) is a system of linear equations that can be written as:

$$\phi - \phi_0 = \begin{pmatrix} [f_1^{\theta_1}(z) + f_2^{\theta_1}(x) + f_3^{\theta_1}(y) + f_4^{\theta_1}(\alpha) + f_5^{\theta_1}(\beta)]|Z_{i1}(\theta_1) \\ \dots \\ \dots \\ [f_1^{\theta_n}(z) + f_2^{\theta_n}(x) + f_3^{\theta_n}(y) + f_4^{\theta_n}(\alpha) + f_5^{\theta_n}(\beta)]|Z_{in}(\theta_n) \end{pmatrix} - \begin{pmatrix} [\sum_{j=1}^5 f_j^{\theta_1}(0)]|Z_{i1}(\theta_1) \\ \dots \\ \dots \\ [\sum_{j=1}^5 f_j^{\theta_n}(0)]|Z_{in}(\theta_n) \end{pmatrix}$$

$$\phi - \phi_0 = J. \begin{pmatrix} \Delta z \\ \Delta x \\ \Delta y \\ \Delta \alpha \\ \Delta \beta \end{pmatrix} \qquad (3)$$

Where ϕ and ϕ_0 are respectively the measured and the residual wavefront vectors. Their coefficients are the values of the system sensing modes. J is the interaction matrix of the system, also called the Jacobian matrix.

Each line of the Jacobian matrix is related to a sensing mode $Z_i(\theta)$, calculated as follow:

$$J = \left(\frac{\Delta Z_i(\theta)}{\Delta z} \quad \frac{\Delta Z_i(\theta)}{\Delta x} \quad \frac{\Delta Z_i(\theta)}{\Delta y} \quad \frac{\Delta Z_i(\theta)}{\Delta \alpha} \quad \frac{\Delta Z_i(\theta)}{\Delta \beta} \right) \qquad (4)$$

Where $\Delta Z_i(\theta)$ corresponds to the Zernike i variation for a misalignment $\Delta z, \Delta x, \Delta y, \Delta \alpha$ or $\Delta \beta$.

The principle of the linear control is to invert the Jacobian matrix [17], the misalignment of L2 is calculated as follow [16]:

$$\begin{pmatrix} \Delta z \\ \Delta x \\ \Delta y \\ \Delta \alpha \\ \Delta \beta \end{pmatrix} = J_{inv}[\phi - \phi_0] \qquad (5)$$

The least square approach of the problem consists in computing the generalized inverse of the matrix J. To do so, we use the singular value decomposition (SVD) [18][,19],[20] of J.

We build J line by line choosing the sensing modes as uncorrelated as possible. The following set of sensing modes is used to experimentally test the linear control code (the results are shown in the next part):
- $Z_5(\theta = 1^\circ)$, $Z_7(\theta = 1^\circ)$, and $Z_8(\theta = 1^\circ)$ for the four corners of the field of view. These sensing modes are sensitive mostly to the x, y, tip, tilt alignment of L2.
- $Z_4(\theta = 0^\circ)$, which is very sensitive to the z position of L2.

III. Experimental results of the linear control alignment

In this part, we test our linear control algorithm on the JOST testbed randomly misaligning L2. We illustrate this paper giving the example of L2 misaligned as follow: +1.3 mm shift along X axis, -0.8mm shift along Y axis, +0.3mm shift along Z axis, +2˚ rotation Y axis, rotation around -1˚ X axis. The alignment correction of testbed is fully automated, this allow us to iterate 3 times for a better correction. Results regarding wavefront quality improvement are shown in Fig.3, the L2 shifts and rotations at the different iterations are shown in Fig.4. The sensing modes choice is detailed in §3.

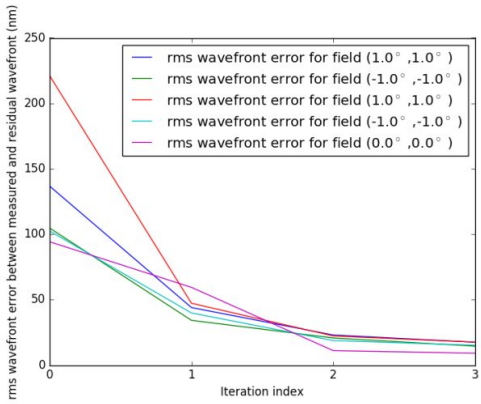

Fig.3 . RMS wavefront error between measured and residual (wavefront error due to the optical design) wavefront. Iteration 0 corresponds to the initial misalignment introduced on L2. We can observe that within 2 iterations, the wavefront error is lower than 20 nm, this fulfills our requirements.

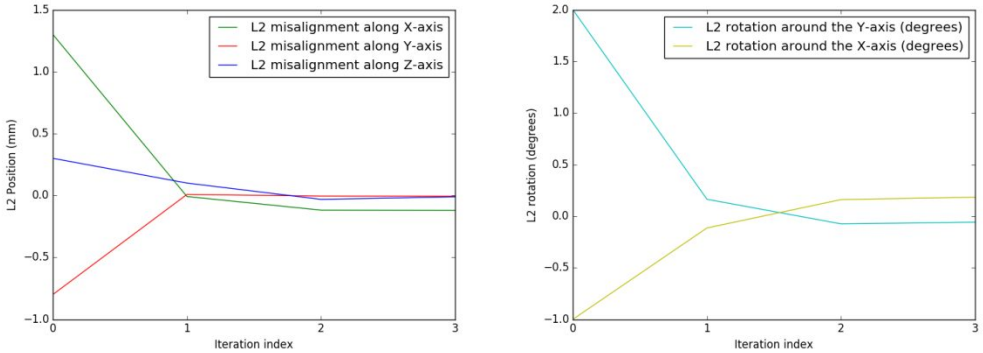

Fig. 4 . L2 position depending on the iteration. Iteration 0 corresponds to the initial misalignment introduced on L2. The position of L2 is corrected after two iterations.

In Fig.4, the plots are converging to the value 0, which means that at each step of the linear control loop, the position of L2 is getting closer to its aligned state. At the same time, the testbed wavefront quality improves and reaches less than 20 nm rms across the field of view at the end.

We can point out that a second iteration is needed to improve the alignment correction because the system is not perfectly linear, we could also investigate on the validity of the very first assumption to neglect the optical path change when such large misalignments occur.

We can conclude that thanks to the automated linear control infrastructure implemented on JOST, the position of L2 can been successfully corrected from random misalignments.

IV. Conclusion

We have achieved the full automation of the JOST testbed, including control of the hardware, data acquisition, calibration, processing for wavefront sensing through focus-diverse phase retrieval, and wavefront control via a linear model. We use Python for high level scripting, and interface from Python to Zemax via Dynamic Data Exchange (DDE) for simulation. Fig. 5 gives an overview of the linear control infrastructure developed for JOST.

The three lenses were initially aligned in x,y and tip-tilt using an alignment telescope, leaving unkown their alignment state along the optical axis. To finalize the alignment of the lenses along the optical axis, we have used a linear control model, similar to the one described above but for these specific control modes. Because only the second lens (secondary mirror surrogate) is motorized, this required tedious manual iterations, and we define our best current state of alignment as our alignment baseline.

We have developed and experimentally validated the linear control infrastructure on the control of L2. We are now about to include the segmented mirror on the testbed for subsequent demonstrations of multi-field control with a segmented telescope. This is a unique aspect of JOST; many other lab wavefront control testbeds are optimized for a single field point (e.g. high contrast AO) or at most for multi-conjugate AO correction of a field about an arcminute across, and often just use DM surface figures to correct wavefront errors. JOST provides a test framework for optical alignment demonstrations for wide-field space telescopes, which requires active control of mirror positions and orientations in three dimensional space.

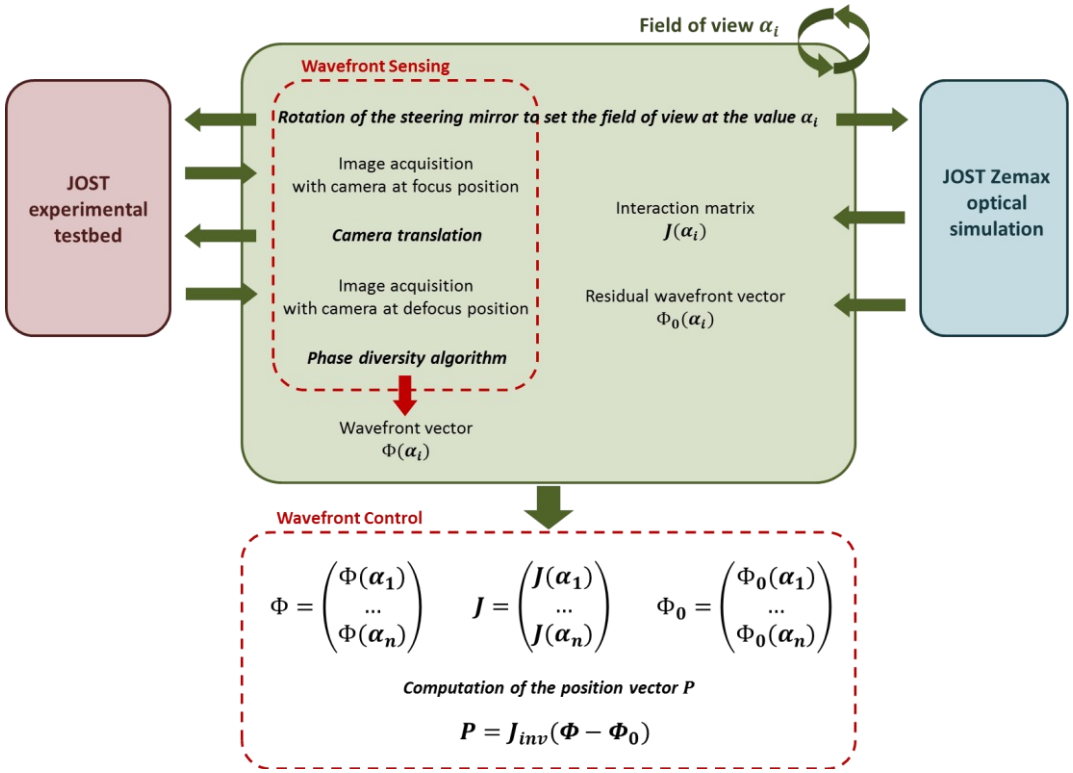

Fig. 5. Different steps of the linear control process. The overall process is handled by Python that will first control the camera for image acquisition, then call IDL for WFS measurements. The WFC computation is based on Python and Zemax, their interaction is managed by the Windows-based dynamic data exchange (DDE) utility. For each experiment, the user is free to choose the fields of view observed, the Zernike modes (sensing modes) and the degrees of freedom (control modes) to include.

The linear control model presented here is directly analogous to the basic strategy proposed for the Multi-Field, Multi-Instrument (MIMF) stage of JWST commissioning. STScI staff will be collaborating with Ball Aerospace and NASA Goddard personnel to execute that stage of commissioning, and JOST provides one venue for gaining additional expertise in preparation for that, alongside the ongoing optical test campaign and rehearsals using software such as Ball's Integrated Telescope Model. In the longer run, there may be more use of JOST to build further confidence in various contingency cases or alternate algorithms, for instance tests to validate the use of non-redundant segment tilts as a backup cophasing strategy. Also, JOST will provide a training platform over years ahead as new staff members rotate onto the telescope team responsible for JWST's continued alignment. The state of the art in wavefront sensing techniques will surely continue to evolve during the perhaps decade-long lifetime of JWST. JOST's flexibility as a general purpose wavefront sensing testbed will allow it to address a wide range of questions or test relevant improved algorithms as needed. This could also include segment phasing strategies for future space missions with larger numbers of segments. The development of such missions, such as the proposed LUVOIR, will be the work of many years.

ACKNOWLEDGMENTS
This work is supported by the JWST Telescope Scientist Investigation, NASA Grant NNX07AR82G (PI: C. Matt Mountain).

REFERENCES
[1] Acton, D. S., Knight, J. S., Contos, A., Grimaldi, S., Terry, J., Lightsey, P., Barto, A., League, B., Dean, B., Smith, J. S., Bowers, C., Aronstein, D., Feinberg, L., Hayden, W., Comeau, T., Soummer, R., Elliott, E., Perrin, M., and Starr, C. W., Wavefront sensing and controls for the James Webb Space Telescope," Space Telescopes and Instrumentation 8442, 84422H-84422H-11 (2012).
[2] Acton, D. S., Towell, T., Schwenker, J., Swensen, J., Shields, D., Sabatke, E., Klingemann, L., Contos, A. R., Bauer, B., Hansen, K., Atcheson, P. D., Redding, D., Shi, F., Basinger, S., Dean, B., and Burns, L., Demonstration of the James Webb Space Telescope commissioning on the JWST testbed telescope," Proc. SPIE 6265 (July 2006).
[3] Acton, D. S., Towell, T., Schwenker, J., Shields, D., Sabatke, E., Contos, A. R., Hansen, K., Shi, F., Dean, B., and Smith, S., End-to-end commissioning demonstration of the James Webb Space Telescope," Proc. SPIE 6687 (Sept. 2007).
[4] Jurling, A. S. and Fienup, J. R., Extended capture range for focus-diverse phase retrieval in segmented aperture systems using geometrical optics," Journal of the Optical Society of America A 31, 661 (Mar. 2014).
[5] Cheetham, A. C., Tuthill, P. G., Sivaramakrishnan, A., and Lloyd, J. P., Fizeau interferometric cophasing of segmented mirrors," Optics Express 20, 29457 (Dec. 2012).
[6] Greenbaum, A. Z., Gamper, N., and Sivaramakrishnan, A., In Focus Phase Retrieval Using JWST-NIRISS' Non-Redundand Mask," Proc. SPIE 9904-159 (July 2016).
[7] Pope, B., Cvetojevic, N., Cheetham, A., Martinache, F., Norris, B., and Tuthill, P., A demonstration of wavefront sensing and mirror phasing from the image domain," MNRAS 440, 125-133 (May 2014).
[8] Perrin, M. D., Soummer, R., and Choquet, _E., James Webb Space Telescope Optical Simulation Testbed I: Overview and First Results," Proc. SPIE 9143, 13 (2014).
[9] Choquet, _E., Levecq, O., N'Diaye, M., Perrin, M. D., and Soummer, R., James Webb Space Telescope Optical Simulation Testbed II: design of a three-lens anastigmat telescope simulator," Proc. SPIE 9143, 91433T (2014).
[10] Egron, E., Levecq, O., N'Diaye, M., Perrin, M. D., and Soummer, R., James Webb Space Telescope Optical Simulation Testbed III: First experimental results with linear-control alignment"Proc. SPIE 9904, 99044A (2016).
[10] Blanc, A., Idier, J., and Mugnier, L. M., Novel estimator for the aberrations of a space telescope by phase diversity," in [UV, Optical, and IR Space Telescopes and Instruments], Breckinridge, J. B. and Jakobsen, P., eds., Proc. Soc. Photo-Opt. Instrum. Eng. 4013, 728-736 (July 2000).
[11] Blanc, A., Fusco, T., Hartung, M., Mugnier, L. M., and Rousset, G., Calibration of NAOS and CONICA static aberrations. Application of the phase diversity technique," Astron. Astrophys. 399, 373-383 (Feb. 2003).
[12] Schechter, P. L. and Levinson, R. S., Generic Misalignment Aberration Patterns in Wide-Field Telescopes,"
Publications of the Astronomical Society of the Paci_c 123(905), 812-832 (2011).
[13] Thompson, K. P., Schmid, T., and Rolland, J. P., The misalignment induced aberrations of TMA telescopes.," Optics express 16(25), 20345-20353 (2008).
[14] Escolle, C., Michau, V., Ferrari, M., Fusco, T., Hugot, E., and Br, Space active optics sensing and control for earth observation at high angular resolution," Proceedings of ICSO (October), 1-6 (2014).
[15] Upton, R., Optical control of the Advanced Technology Solar Telescope," 45(23), 5881-5896 (2006).
[16] Acton, D. S. and Knight, J. S., Multi-field alignment of the JamesWebb Space Telescope," Space Telescopes
and Instrumentation 8442, 84423C (2012).
[17] Strang, G., [Linear Algebra and Its Apllications] (2010).
[18] Quiros-pacheco, F., Conan, J.-m., and Petit, C., Generalized aliasing and its implications in modal gain optimization for multi-conjugate adaptive optics," Journal of the Optical Society of America A 27(11), 182-200 (2010).
[19] Chapman, H. N. and Sweeney, D. W., Rigorous method for compensation selection and alignment of microlithographic optical systems," Proc. SPIE 3331, 102-113 (1998).
[20] Acton, D. S. and Knight, J. S., Multifield alignment of the James Webb Space Telescope," Proc. SPIE 8442, 84423C (Sept. 2012).